Investigating Microscopic Flow within Different Channel Geometries using a Leica DMI4000 Inverted Microscope

Anusha Fatima Alam (PRA 0101)

1. Introduction

Observing fluid flow through microchannels of different shapes and sizes is integral to understanding the intricate behavior of fluids at a microscopic level. This has vast and diverse practical applications from developing biological microchips, to modern DNA sequencing and understanding blood flow.

The primary objective of this report is to examine the fluid flow of different microchannels consisting of a sharp and smooth bend and a sharp and gradual opening. A Leica DMI4000 Inverted Microscope was utilized to analyze streaklines for different geometries to assess the experimental parameters like the velocity profile relative to varying parameters like distance from the sidewalls, the height of reservoir.

Two fundamental equations of fluid mechanics that will be utilized throughout this report to analyze microscopic flow are the conservation of mass equation and Bernoulli's equation which have been described below. The conservation of mass equation can be modelled by:

$$\dot{m}_{in} - \dot{m}_{out} = \dot{m}_{acc}$$

where $\dot{m}_{in}$ is the mass flow rate at the inlet, $\dot{m}_{out}$ is the mass flow rate at the outlet and $\dot{m}_{acc}$ is the mass flow rate accumulated. However due to conservation of mass, $\dot{m}_{acc} = 0$; hence the equation can be rearranged to $\dot{m}_{in} = \dot{m}_{out}$. For an incompressible fluid, and a uniform velocity field this equation can be revised to:

$$\rho U_A S_A = \rho U_B S_B$$

where ρ is the density of the fluid, U_A and U_B are the velocity at point A and point B respectively, and S_A and S_B are the cross-sectional area at point A and point B respectively. Using the Bernoulli's equation, the relationship between the height, pressure, and velocity at two points can be given by:
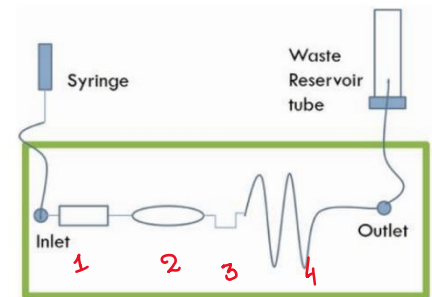
$$P_B + \frac{1}{2}\rho U_B^2 + \rho g z_B = P_A + \frac{1}{2}\rho U_A^2 + \rho g z_A \quad [1]$$

These two governing equations will be used later throughout the report for calculations and data processing.

2. Experimental Procedure

The procedure outlined in the Microfluidics lab manual [2] was followed, however certain adaptations and adjustments were made to minimize the impact of instrumental uncertainties and potential human error.

Figure 1: Annotated Microfluidic Chip Diagram (with four different microchannels) [2]

2.1 Experimental Set-up: To experimentally examine the behavior of fluid flow within different microchannels, a microfluidic chip was placed on the platform of the Leica DMI4000 Inverted Microscope, where the fluid entered from the syringe, passed through the chip and exited to the reservoir. The stage height and orientation was adjusted to align with the microfluidic chip with the respective microchannel. The microfluidic chip consists of 4 different
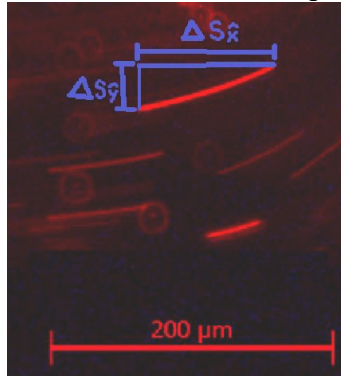
microchannels (refer to figure 1) with different geometries: an abrupt opening, a gradual opening, a sharp bend and a smooth bend. The microscope camera was used to capture images of the streaklines of the flowing fluid by observing the trajectory of the diluted fluorescent beads (via the LAS software).

2.2   Adjustments and Adaptations: The abrupt opening (Channel 1) and the gradual opening (Channel 2) were captured with an objective lens of magnification 10x, whilst the sharp bend (Channel 3) and the smooth bend (Channel 4) were observed under a magnification of 20x. This adaptation was made to account for the fact that channels 3 and 4 were relatively smaller than channels 1 and 2, which made it difficult to observe sharp and clear streaklines. By adjusting the Gamma, grain, and opacity of the images, streaklines with high velocities were made more distinct and clearer, without the need of changing the height between different microchannels.

2.2   Length Conversion: Microsoft Paint was used to determine the pixel length of each streakline by recording the pixels ($\Delta Pixel$) in the x and y direction of each streak and using Pythagoras theorem to determine the length (Δs) of each streak. The physical length scale of each image captured by the LAS software was a standard of $200\ \mu m$ given on the on-screen scale of each image. The length scale in terms of the numbers of pixels was 217 pix. Therefore, the length to pixel quotient (i.e. the magnification scale, Q) was $0.922\ \mu m/pix$ for each image. The displacement in the î-direction is:

$$\Delta s_{\hat{\imath}} = \Delta Pixel_{\hat{\imath}} \times \frac{Physical\ Length}{Pixel} = \Delta Pixel_{\hat{\imath}} \times Q$$

Using Pythagoras theorem, the length of each streak is given by $\Delta s = \sqrt{\Delta s_{\hat{x}}^2 + \Delta s_{\hat{y}}^2}$. The velocity of each streak can then be computed by: $U = \frac{\Delta s}{\Delta t}$, where Δt is the exposure time. Refer to sample calculations below computed for streak observed in figure 2:

The pixel length in the x and y direction was determined from Microsoft paint as $\Delta Pixel_{\hat{x}} = 134 \pm 2\ pix$ and $\Delta Pixel_{\hat{y}} = 43 \pm 2\ pix$. Therefore:

$$\Delta s_{\hat{x}} = \Delta Pixel_{\hat{x}} \times Q = 134 \times 0.922 = 123.548\ \mu m$$
$$\Delta s_{\hat{y}} = \Delta Pixel_{\hat{y}} \times Q = 43 \times 0.922 = 39.646\ \mu m$$

$$\Delta s = \sqrt{\Delta s_{\hat{x}}^2 + \Delta s_{\hat{y}}^2} = \sqrt{123.548^2 + 39.646^2} = 129.753\ \mu m$$

The exposure time, Δt, for this streak was 48.2 ms. Therefore the velocity for this streakline can be computed using:

$$U = \frac{\Delta s}{\Delta t} = \frac{129.753\ \mu m}{48.2\ ms} = 2.692\ \mu m/ms$$

Figure 2: *An image of a Streakline across a gradual opening (channel 2) microchannel*

For the sake of consistency, for each of the trials for each microchannel, the brightness and the defined origin (i.e., the height) was kept constant. Different velocities for specific heights were recorded and then averaged to minimize the impact of random errors.

3. **Uncertainty Propagation and Analysis:**

The experimental results demonstrate the application of the two governing equations (the conservation of mass and Bernoulli's equation) to understand fluid behavior within microchannels of different geometries. Although the experimental set-up produced relevant and sufficient results that corroborate the theoretical model, nevertheless, there are significant sources of uncertainties and

errors that could have potentially minimized the accuracy and precision of the calculations. For this laboratory, the major sources of error arise from instrumental uncertainties. This is because every reading taken from the apparatus had an associated uncertainty. The absolute uncertainty in the exposure time is $\delta_{\Delta t} = \pm 0.1 \, ms$. And the absolute error in the pixel readings from Microsoft Paint is $\delta_{\Delta s_i} = \pm 2 \, pix$ in both the x and the y directions and the scale. Therefore, the uncertainty propagation

for the length $\delta_{\Delta s_i}$ in the î-direction is given by: $\delta_{\Delta s_i} = \Delta s_i \sqrt{(\frac{\delta_{\Delta s_i}}{\Delta s_i})^2 + (\frac{\delta_Q}{Q})^2}$

where δ_Q is the uncertainty in length to pixel scale quotient which comes from the uncertainty in the pixel length of the on-screen reading scale. Fractional uncertainties in each reading is considered.

The overall uncertainty in $\sigma_{\Delta s}$ is: $\delta_{\Delta s} = \Delta s \sqrt{(\frac{\delta_{\Delta s_{\hat{x}}}}{\Delta s_x})^2 + (\frac{\delta_{\Delta s_{\hat{y}}}}{\Delta s_y})^2}$

The uncertainty in velocity is then given by: $\delta_U = U \sqrt{(\frac{\delta_{\Delta s}}{\Delta s})^2 + (\frac{\delta_{\Delta t}}{\Delta t})^2}$

The uncertainties have been propagated below with sample calculations for the streak line shown above in figure 2.

$$\delta_{\Delta s_{\hat{x}}} = 123.548 \sqrt{(\frac{2}{134})^2 + (\frac{2}{217})^2} = 2.167 \, \mu m$$

$$\delta_{\Delta s_{\hat{y}}} = 39.646 \sqrt{(\frac{2}{43})^2 + (\frac{2}{217})^2} = 1.879 \, \mu m$$

$$\delta_{\Delta s} = 129.753 \sqrt{(\frac{2.167}{123.548})^2 + (\frac{1.879}{39.646})^2} = 6.557 \, \mu m$$
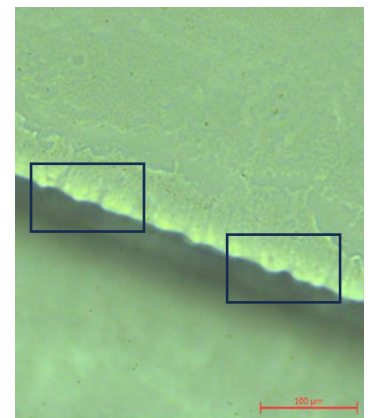
$$\delta_U = 2.692 \sqrt{(\frac{6.557}{129.753})^2 + (\frac{0.1}{48.2})^2} = 0.136 \, \mu m/ms$$

Therefore, the velocity for the streak line in figure 2 is $2.692 \, (\pm 0.136) \, \mu m/ms$. Because the experimental uncertainties were relatively smaller than the instrumental uncertainties, only the major source of error is accounted for, and therefore the instrumental uncertainties are used to draw the error bars on the graphs. Nevertheless, it is important to acknowledge that there is also potential for human error especially in the choice and clarity of streaks and images, the ability to distinguish where a streak begins and terminates and the choice of software to interpolate the pixel length. These non-quantifiable human errors could also contribute to errors the accuracy of calculations.

4. Results and Discussion

4.1   Chip Design: A picture (refer to figure 3) of the straight channel was taken under 40x magnification where minor imperfections in the channel sidewalls were perceptible.

Figure 3: An image of the channel sidewalls taken with LAS software under 40x magnification

These imperfections arise due to lack of perfect smoothness of the walls which introduced surface roughness and an asymmetric pattern at the surface level of the walls. These variations were enhanced at the extremes of the walls, for instance at the corners of a channel with the sharp bend. Although
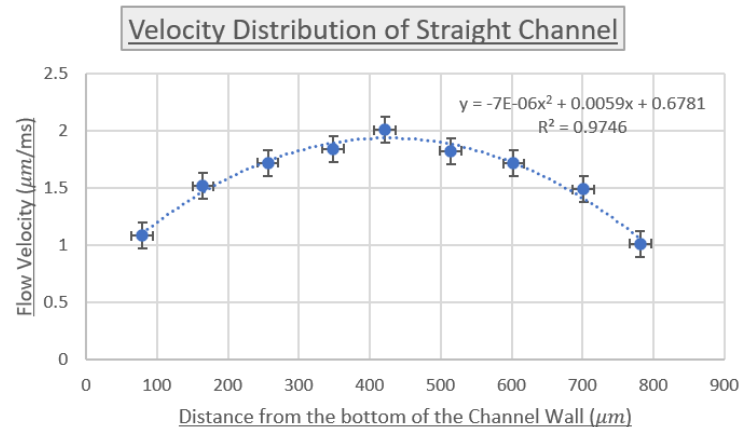
these imperfections were subtle, they were significant enough to impact the fluid flow and the velocity behavior. As such, it is prudent to acknowledge this while evaluating the results obtained from the experiment. After closely examining these ridges, each ridge appears to have a maximum depth of 9 μm. Compared to the width of channel, the maximum depth of each ridge is significantly smaller and hence it is only appreciable near the walls where it introduces minor turbulence at the walls. As such, this effect of ridges on fluid flow can be neglected at the center of streamtube where flow is relatively unaffected.

4.2   Straight Channel:

The wide straight channel (channel 1) was observed to derive a velocity profile and examine the effect of syringe height on the velocity. The maximum velocity is expected to occur at the centre of the channel because of an expected parabolic velocity distribution. This is because the center of the stream tube is the least subject to turbulence and friction caused by the wall surface. Whilst the largest velocity gradient is expected to occur near the walls of the channel because of the no-slip condition and imperfections at the surface which yields the largest velocity gradient between the channel walls and the channel centre. The velocity profile experimentally determined at different distances from the channel side is visualized in figure 4. The error bars for each point are determined using the uncertainty propagation shown in section 3.

Distance from bottom of the Channel Wall (μm)	Velocity ($\mu m/ms$)
79.4 $\pm$ 15.2	1.085 $\pm$ 0.152
164.8 $\pm$ 12.4	1.517 $\pm$ 0.128
256.3 $\pm$13.1	1.721 $\pm$ 0.149
348.7 $\pm$ 11.6	1.847 $\pm$ 0.132
421.3 $\pm$ 9.3	2.011 $\pm$ 0.158
514.2 $\pm$ 22.3	1.825 $\pm$ 0.122
602.9 $\pm$ 17.2	1.717 $\pm$ 0.124
701.3 $\pm$ 19.2	1.493 $\pm$ 0.111
781.5 $\pm$ 13.4	1.013 $\pm$ 0.142

Table 1: *Distance from Wall Vs. Flow Velocity*

Velocity Distribution of Straight Channel

$y = -7E-06x^2 + 0.0059x + 0.6781$
$R^2 = 0.9746$

Flow Velocity ($\mu m/ms$)

Distance from the bottom of the Channel Wall (μm)

Figure 4: *Velocity Distribution of a Wide Straight*

The velocity profile is expected to be parabolic in nature because it maximum at the center and the largest velocity gradient lies the extremes of the walls. As such the graph obtained in figure 4 corroborates this parabolic nature of velocity. It is clear that the velocity increases as a function of squared distance from the channel wall. This corroborated by the fact that the coefficient of determination is extremely close to 1 being 0.946. Additionally observing the graph, it very evident that residuals of this curve are extremely small, and the data lies extremely close to the line of best fit. The existence of residuals are a result of the limitations of camera and the experimental set-up.

The velocity of syringe can also be manipulated by adjusting the height of the syringe. Under the assumption that the fluid is incompressible, an increase in the height will increase the gravitation potential energy of the fluid and will also increase the kinetic energy which consequently increases the

flow velocity. Assuming that the relative height microfluidic chip is zero and the syringe remains stationary, the Bernoulli equation can be rewritten as:

$$\frac{1}{2}\rho U_B^2 = \rho g z_A \quad \rightarrow \quad U_B = \sqrt{2gz_A}$$

Or alternatively, $z_A = \frac{U_B^2}{2g}$

The theoretical model derived above indicates that there exists a square-root relationship between the velocity of the fluid in terms of height. Alternatively, there is a parabolic velocity for height in terms of fluid velocity. For consistency, the velocity measurements were taken at the center of the stream tube for all heights to avoid the impact of minor turbulence and disturbances at the edge of channel walls.

Figure 5: *Parabolic Distribution of Height Vs. Fluid Velocity. Horizontal errors bars arise from uncertainty in height ($\pm 0.5\ mm$) and vertical error bars were computed uncertainty calculations in section 3.*

This relationship was also experimentally (see figure 5) observed by manually adjusting the height of the syringe at regular intervals. However, it is important to note that this experimental relationship is not consistent with the theoretical model. The theoretical model predicts that there is a square-root relationship, however the experimental results yield a parabolic relationship. This inconsistency could plausibly exist because the flow was not perfectly incompressible and there may potentially exist viscous forces which were more perceptible in a narrow channel flow.

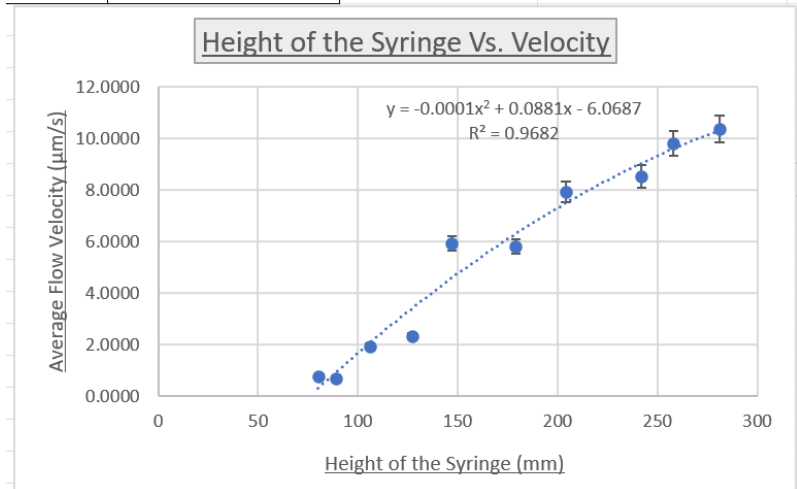*Figure 6:* *Gradual Transition in Channel, Abrupt Channel is equivalent to the straight channel*

4.3   Channel of Different Size:

Channels of different sizes can introduce either sudden abrupt or smooth and gradual change in the width of the channel which affects the behavior of how the fluid flows through the inlet. To model the impact of the width of the channel on its velocity assuming the channel depth is constant, and the cross-section of the channel is rectangular, we rearrange the conservation of mass equation: $U_B = U_A \frac{S_A}{S_B} = U_A \frac{w_A}{w_B}$
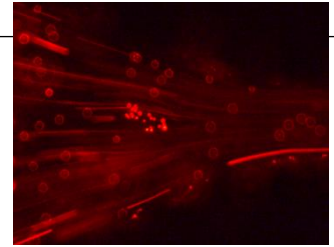
This rearrangement of the conservation of mass equation can be used to predict the exit velocities based on the based on the initial velocities of the stream (refer to table 2 for calculations).

Type of Channel	Initial Channel Width (μm)	Exit Channel Width (μm)	Initial Velocity ($\mu m/ms$)	Theoretical Exit Velocity ($\mu m/ms$)	Actual Exit Velocity ($\mu m/ms$)
Abrupt (Converging)	875 ± 4	238 ± 5	0.286 ± 0.052	1.051 ± 0.211	1.623 ± 0.028
Gradual (Diverging)	249 ± 6	619 ± 4	5.325 ± 0.142	2.142 ± 0.156	1.324 ± 0.038

Table 2: *Theoretical and Actual Velocity determined based on Channel Parameters*

Examining table 2 above, actual velocities for both the abrupt and gradual change lie outside the theoretical values and its quantified uncertainty tolerances. This could be due to the sources of non-quantifiable human errors and lack of repetition of trials where anomalies couldn't be eliminated. The gradual transition channel observes an increase in velocity of approximately 92 % per 10 μm, whilst the abrupt channel observes an increase of roughly 63 % per 10 μm. This is not surprising because more disturbances and turbulences are observed in the abrupt channel rather than the gradual transition. As such in the abrupt transition more fluid hits the wall perpendicularly, momentarily becoming static. From this it can be concluded that gradual transitions appear to be more energy efficient requiring lower initial velocity to obtain a similar final velocity. For practical purposes in real-life this can be extremely useful in increasing and decreasing fluid velocity, for example in blood flow or through pipelines or other industrial applications.

4.4   Channels of Different Bends:

Figures 7 and 8 depict the pathlines of the flow within a smooth and sharp bend respectively. Around the smooth bend (channel 4) the initial velocity was determined to be 19.453 ($\pm$ 2.431) μm/ms, whilst the exit velocity was determined to be 14.934 ($\pm$ 1.124) μm/ms. As such, the smooth bend observed a decrease in velocity of roughly 23.2 %. On the other hand, the sharp bend (channel 3) had an initial velocity of 24.823 ($\pm$ 0.921) μm/ms and an exit velocity of 16.848 ($\pm$ 1.358) μm/ms. There, the sharp bend observed a decrease in velocity of approximately 32.2 %. For the smooth bend, the flow is more laminar, however for the sharp bend small turbulences are introduced at the corner of the bends especially near the walls were the fluid becomes more and more static.
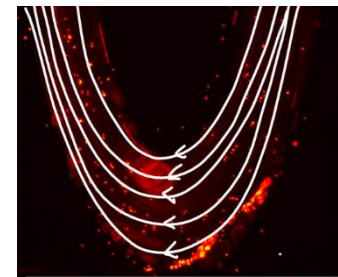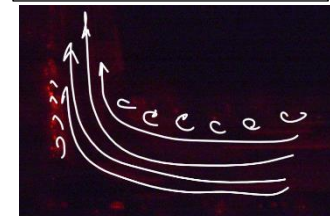

**Figure 7:** Smooth Bent

Figure 8: Sharp Bent

5. **Conclusion** Ultimately, primary objective of this report to explore the application of the two governing equations, namely the conservation of mass and Bernoulli equation, was successfully achieved. The behaviour of flow through 4 different microchannels was successfully observed. A velocity distribution was obtained at different proximities from the channel wall, which verified the existence of viscous forces. Additionally measuring the effect of syringe height on the velocity at the center, produced results that contradicted the theoretical model of the square-root relationship. By examining different microchannels it can be concluded that the geometry certainly does impact the fluid flow and behavior which can motivate the use of a certain geometry over one another based on the desired applications.

6. **References**

[1] "14.8: Bernoulli's Equation." *Physics LibreTexts*, Libretexts, 14 Dec. 2022, phys.libretexts.org/Bookshelves/University_Physics/Book%3A_University_Physics_(Ope nStax)/Book%3A_University_Physics_I_Mechanics_Sound_Oscillations_and_Waves_(Op enStax)/14%3A_Fluid_Mechanics/14.08%3A_Bernoullis_Equation#:~:text=p1%2B12%C F%81,follow%20it%20along%20its%20path.). Accessed 2 Dec. 2023.

[2] Deng, P., & Lu, Z. (2023-2024). Microfluidics Lab Manual. Toronto, ON: University of Toronto. Accessed 2 Dec. 2023.

Appendix A: Optional Analysis (Bonus Question)

BONUS QUESTION: This optional analysis can be included as an APPENDIX to your main report that does not affect page count, but please keep this section short (max one page). Ignoring this section will not affect your lab report grade, but a good answer can increase it! Think back to the results you observed as velocity changed with the syringe height and channel width. Can you derive a theoretical model for these observed relationships?

Hint: Consider the following idealized experimental setup shown in Figure 3. Point 1 is the free surface of the fluid in the syringe. Point 2 is a location inside the microfluidic chip channel. Point 3 is the exit of the tubing out of the microfluidic chip. Both point 1 and point 3 are exposed to atmospheric pressures and temperatures. Channel areas S1, S2, S3, and heights z1, z2, and z3 (z2 = z3) are known parameters. You can assume S1 ≫ S3. Using Bernoulli's equation, first find the relationship between U3 and z1 (refer to derivation of Torricelli's law), then use conservation of mass to relate U2 to U3, and subsequently find the relationship between U2 and z1. Are you able to derive the proportionality relationship and coefficient you observed earlier between the velocity inside the microfluidic channel (U2) and the syringe height (z1)? If they differ, think about whether the assumptions we made in our theoretical model are valid.

$P_1, U_1, S_1, \rho g z_1 \rightarrow$

$P_3, U_3, S_3, \rho g z_3$ $P_2, U_2, S_2, \rho g z_2$
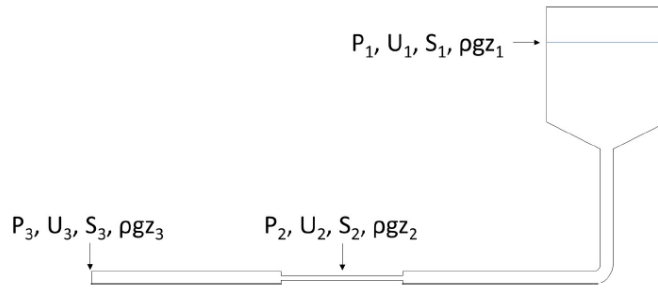
1) Bernoulli's Equation

$$P_1 + \frac{1}{2}\rho U_1^2 + \rho g z_1 = P_2 + \frac{1}{2}\rho U_2^2 + \rho g z_2$$

P_1 and P_2 are both exposed to atmospheric pressure.

$$Therefore\ P_1 = P_3\ and\ z_2 = z_3.$$

$$\frac{1}{2}\rho U_1^2 + \rho g z_1 = \frac{1}{2}\rho U_3^2 + \rho g z_2$$

$$U_3 = \sqrt{2g\ (z_1 - z_2)}$$

2) Conservation of Mass

$$\dot{m} = \rho A U$$

$$\rho U_1 S_1 = \rho U_2 S_2$$

Assuming S_1 is much greater than S_3 and A_1 is much greater than A_2. We can approximate that $U_3 \approx U_2$.

$$U_2 = \frac{A_1}{A_2}\sqrt{2g\ (z_1 - z_2)}$$

Where K $== \frac{A_1}{A_2}\sqrt{2g}$ is the constant of proportionality.